Strategies for Controlling the Planar Arrangement of Block Copolymer Micelles and Inorganic Nanoclusters

Ryan D. Bennett,[†] Andrew C. Miller,[†] Naomi T. Kohen,[‡] Paula T. Hammond,[†] Darrell J. Irvine,[‡] and Robert E. Cohen*,[†]

Department of Chemical Engineering and Department of Materials Science and Engineering and the Biological Engineering Division, Massachusetts Institute of Technology, 77 Massachusetts Avenue, Cambridge, Massachusetts 02139

Received August 23, 2005; Revised Manuscript Received October 17, 2005

ABSTRACT: We report several strategies for varying the diameter, the center-to-center spacing, and the areal density of block copolymer micelles, or inorganic nanoclusters synthesized in the cores of the micelles, on planar substrates. The amphiphilic block copolymer, poly(styrene-*b*-acrylic acid) (PS/PAA), forms micelles in toluene solution that can be spin-coated onto a substrate to create quasi-hexagonal arrays of spherical PAA domains within a PS matrix. The carboxylic acid groups within the PAA domains can be utilized in a nanoreactor synthesis scheme to create inorganic nanocluster arrays, or the PAA domains can be cavitated to expose the carboxylic acid groups to the surface for possible covalent coupling reactions. The strategies we use to vary the planar arrangements include variation of the molecular weight of PS/PAA, variation of the amount of metal loaded into the micellar solution, addition of PS homopolymer into the micellar solution, and the mixing of different micellar solutions. Through these routes, we demonstrate varying the diameter of the inorganic nanoclusters from 4.7 to 16 nm and the areal density from 8×10^{10} to 6.5×10^{9} nanoclusters cm^{-2}. We are also able to create arrays of nanoclusters containing more than one inorganic species, with each nanocluster containing either one or all of the inorganic species, depending on the sequence of processing conditions employed. We characterize these arrays using energy-dispersive X-ray analysis on a scanning transmission electron microscope.

Introduction

In the past decade, the use of self-assembling systems for the fabrication of materials on the nanometer scale has been an active area of research,[1] with possible applications in areas such as data storage, electronics, and molecular separation.[2] Block copolymers thin films are nanoscale self-assembling systems[3−8] that have been exploited due to their intrinsic nanometer feature size, their ease of synthesis, and their rich phase behavior.[9,10] Block copolymer lithography[3] is an example that uses the heterogeneous morphology of block copolymer thin films to transfer periodic arrays of features onto a substrate on a nanometer length scale. Generally, solvent cast block copolymer films are annealed on the substrate to generate an equilibrium morphology and to reduce the occurrence of unwanted grain boundaries and other defects.

A related but different route for patterning on the nanoscale utilizes amphiphilic block copolymer micellar solutions to produce ultrathin nanostructured films. These micellar systems, which have frequently been based on poly(styrene-*block*-2-vinylpyridine), have been utilized for various applications, including nanolithography based on gold-loaded micelles,[11] deposition of gold nanocluster arrays for ZnO nanowire growth[12] and protein binding,[13] deposition of ZnO nanoclusters arrays for optical devices,[14] and deposition of iron oxide nanocluster arrays for carbon nanotube growth[15] and magnetic applications.[16] Previous work in our research group used block copolymer micellar thin films based on poly(styrene-*block*-acrylic acid) to create arrays of PAA domains that could be cavitated to expose free carboxylic acid groups.[17] These systems have been used to generate planar arrays of various inorganic nanoclusters,[17] including iron oxides suitable for catalyzing carbon nanotube growth.[18] One advantage of the micellar route to generate such planar nanoarrays arises from the fact that these systems are often trapped in a nonequilibrium state, facilitating the opportunity to vary structural parameters such as the characteristic shape, size, and spacing of the array features.

In this paper, we focus on strategies to vary the size and spacing of spherical block copolymer micellar domains on planar surfaces as well as routes that allow for nanocluster synthesis within the spherical domains. Our specific approach capitalizes on the ability of the amphiphilic block copolymer, poly(styrene-*block*-acrylic acid) (PS/PAA), to form quasi-hexagonal planar arrays of PAA spheres in a matrix of PS. As shown previously,[17,18] it is possible to exploit the metal-binding properties of the carboxylic acid groups in chemical synthesis schemes that are confined to nanometer-scale reaction zones. Application of these nanoreactor synthesis protocols ideally requires a measure of control over the size, spacing, and packing arrangement of these reaction zones on the planar substrate. The present work addresses some of these issues using a variety of strategies, including varying the block copolymer molecular weight, adding homopolymer of PS into the micellar solution, and also by the combination of different micellar solutions.

We also report a novel route for creating metal nanocluster arrays containing more than one inorganic species, with each nanocluster containing either one or all of the inorganic species, depending on the conditions of the synthesis. In previous research in this area, Sohn

[†] Department of Chemical Engineering.
[‡] Department of Materials Science and Engineering and the Biological Engineering Division.
* To whom correspondence should be addressed: e-mail recohen@mit.edu.

10.1021/ma0518555 CCC: $30.25
Published on Web 11/15/2005

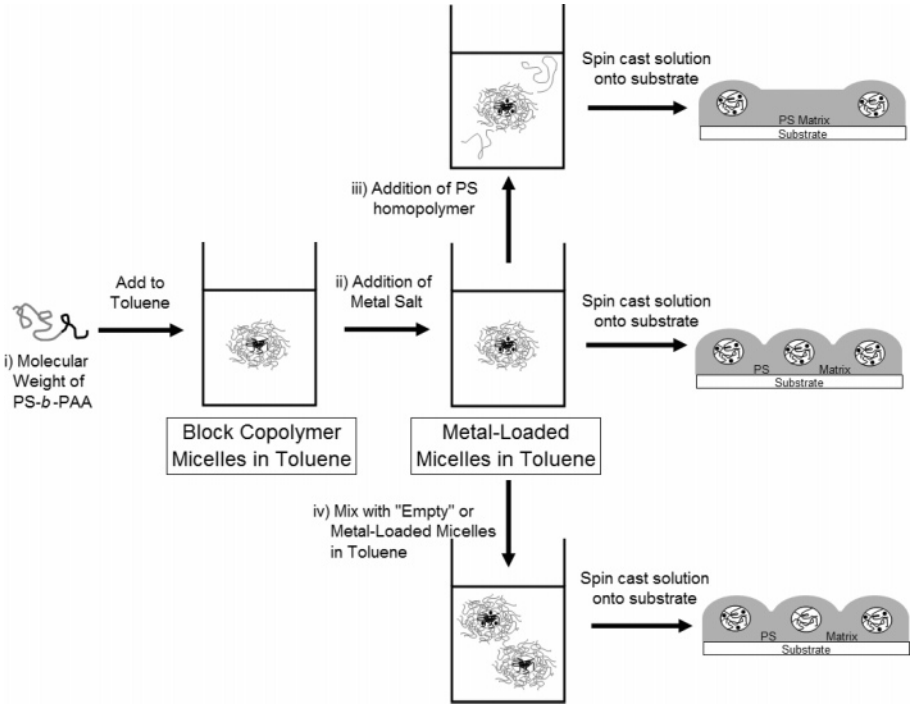

Figure 1. Diagram of synthesis procedures for modification of block copolymer micellar thin films.

and co-workers developed a route to create arrays containing two different species of nanoclusters by combining presynthesized nanoparticles with metal-loaded block copolymer micelles in solution.[19] In contrast, our more general route focuses on the time-dependent interdiffusion of inorganic species following mixing of micelle solutions that have been previously loaded with different inorganic species. These arrays are characterized using energy-dispersive X-ray (EDX) analysis on a scanning transmission electron microscope (STEM).

Experimental Section

Materials. Three PS-*b*-PAA copolymers were used in this work, with molecular weights and nomenclatures as follows: PS/PAA (16.4/4.5) [M_n(PS) = 16 400 g/mol, M_n(PAA) = 4500 g/mol, PDI = 1.05]; PS/PAA (66.5/4.5) [M_n(PS) = 66 500 g/mol, M_n(PAA) = 4500 g/mol, PDI = 1.07]; and PS/PAA (11.0/1.2) [M_n(PS) = 11 000 g/mol, M_n(PAA) = 1200 g/mol, PDI = 1.11]. The copolymers were used as received from Polymer Source, Inc. The synthesis procedure and characterization of the copolymers are included in the Supporting Information. A homopolymer of polystyrene (PS) (M_n = 8500 g/mol, PDI = 1.06) was used as received from Polymer Source, Inc. The following chemicals were also used as received: anhydrous iron(III) chloride ($FeCl_3$) obtained from Sigma-Aldrich Co., lead(II) acetate trihydrate ($PbAc_2$) obtained from Sigma-Aldrich Co., sodium hydroxide (98.9%) obtained from Mallinckrodt, and toluene (HPLC grade, 99.8%) obtained from Sigma-Aldrich Co.

The silicon nitride membrane window substrates were purchased from Structure Probe, Inc. Each substrate (surface area ~ 4.5 mm^2) consisted of a 100 nm thick amorphous, low-stress Si_3N_4 membrane supported on a 0.2 mm thick silicon wafer that had been back-etched in the center to create the electron transparent Si_3N_4 window (surface area ~ 0.2 mm^2). The use of the electron-transparent silicon nitride substrates allows for direct TEM characterization without disturbing the spin-cast films. Each substrate was rinsed with toluene prior to film casting. All aqueous solutions were made using deionized water (>18 MΩ cm, Millipore Milli-Q).

Sample Preparation. To produce the metal-loaded micellar arrays, we employed a variety of synthesis procedures that capitalize on the micellar organization of PS/PAA in toluene solution. A summary of the processing routes is shown in Figure 1 and outlined below.

In route i, three different molecular weights of PS/PAA (listed in the Materials section) were mixed with toluene at a concentration of 12.5−15 mg/mL. For the case of PS/PAA (16.4/4.5), the solution initially appeared slightly cloudy. After heating this solution to ~145 °C for 20 min, the solution became optically clear, and it remained clear after cooling to room temperature. Previous work[17] has shown that this transition in solution optical properties is the result of a change from (equilibrium) cylindrical to (kinetically trapped) spherical block copolymer micelles. For the case of PS/PAA (11.0/1.2) and PS/PAA (66.5/4.5), the same heating and cooling procedure was followed, and optically clear final solutions were obtained. The as-prepared solutions for these two copolymers were much less cloudy than the initial PS/PAA (16.4/4.5) solution. The PAA micelle cores were selectively loaded with the chosen metal by adding the metal species to the micellar solution at a ratio of 5.4 metal ion equivalents per carboxylic acid group (metal loading ratio). Thin films were then created by spin-casting the metal-loaded micellar solutions onto the planar substrates at between 6000 and 8000 rpm for 1 min at room temperature.

In route ii, PS/PAA (16.4/4.5) was mixed with toluene at a concentration of 12.5−15 mg/mL. The chosen metal was then added at three different metal loading ratios (0.3, 5.4, and 15). Thin films of each solution were then produced by spin-casting the solution onto the substrates.

In route iii, PS homopolymer (M_n = 8500 g/mol) was added to the micellar solutions (metal loading ratio 5.4) based on the PS/PAA (16.4/4.5) system. Homopolymer was added in quantities leading to solutions in which the molar ratio of molecules of PS homopolymer to PS/PAA block copolymer [PS: PS/PAA] was equal to 4 and 10, respectively. To reduce the viscosities of these solutions to acceptable levels for spin-casting, the solutions were diluted with toluene from 13 mg of PS/PAA/mL of toluene to 5 mg of PS/PAA/mL of toluene. Thin films were then produced by spin-casting these solutions onto substrates.

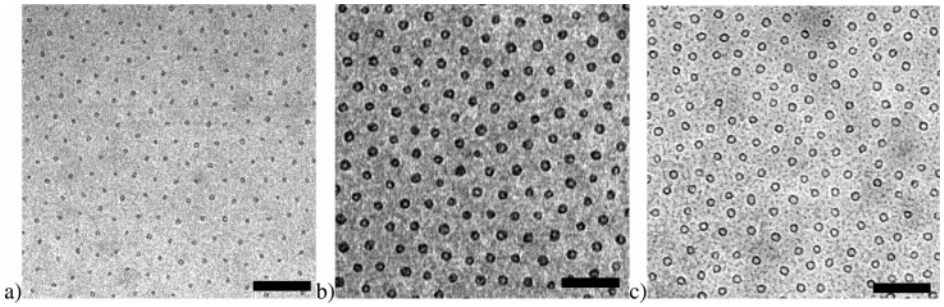

Figure 2. TEM images of iron oxide nanocluster arrays synthesized from micellar thin films using PS/PAA (16.4/4.5) with an $FeCl_3$ loading ratio of (a) 0.3, (b) 5.4, and (c) 15. Scale bar = 100 nm.

Table 1. Effects of Varying Metal Loading Ratio on Diameter, Center-to-Center Spacing, and Areal Density of Iron Oxide Nanocluster Arrays.

PS (g/mol)	PAA (g/mol)	metal loading ratio	diameter (nm)	C-to-C spacing (measured)[a] (nm)	(FFT)[b] (nm)	areal density (parts/cm^2)
16 400	4500	0.3	8 ± 0.7	39.6 ± 4.1	35.8	8.2×10^{10}
16 400	4500	5.4	16.0 ± 1.6	44.9 ± 4.0	39.5	6.0×10^{10}
16 400	4500	15	$162. \pm 1.1$	44.8 ± 4.2	38.1	6.3×10^{10}

[a] From TEM images. [b] Determined from fast Fourier transform (FFT) of TEM image.

In route iv, metal-loaded micellar solutions were combined with either an unloaded micellar solution (micelle solution that bypassed the metal loading step) or a micelle solution that had been loaded with a different metal species. In the first example, a micelle solution of PS/PAA (16.4/4.5) with a metal loading ratio of 5.4 was mixed in a 1:1 volume ratio with an unloaded micelle solution of the same PS/PAA copolymer. After the combined solutions had been mixed for 1 min, a thin film was spin-cast onto a substrate. In the second example, a micelle solution of PS/PAA (16.4/4.5) with an $FeCl_3$ loading ratio of 0.3 was mixed in a 1:1 volume ratio with a micelle solution of PS/PAA (16.4/4.5) with a $PbAc_2$ loading ratio of 0.9. Thin films were then created by spin-casting this mixed micellar solution onto a substrate after mixing the solutions for a short time (2 min) and an extended time (120 h).

In each of the routes above, there exists the possibility of bypassing the metal loading step (step ii in Figure 1) to create arrays of PAA domains within a PS matrix. From previous research it is known that treating these films in a basic solution containing a monovalent cation results in significant swelling of the PAA domains,[17] which eventually leads to localized cavitation that exposes the interior of the PAA domains to the surface.

In each of the routes listed above, the polymer thin film was removed by oxygen plasma etching (rf plasma, 8−12 MHz) for 15 min, leaving only the inorganic species remaining on the substrate. The inorganic nanocluster arrays were then characterized using TEM, atomic force microscopy (AFM), and STEM.

Microscopy and Spectroscopy. TEM was performed on a JEOL 200CX operating at 200 kV and a JEOL 2000FX operating at 200 kV. STEM was performed on a VG HB603 operating at 250 kV. AFM was performed on a Digital Instruments Dimension 3000 Nanoscope IIIA scanning probe microscope operating in tapping mode using a silicon cantilever. Dynamic light scattering (DLS) was performed on a BI-9000AT digital autocorrelator (Brookhaven Instruments Corp.) using a 514 nm laser, at $\theta = 90°$ and a temperature of 25 °C. X-ray photoelectron spectroscopy (XPS) was performed with a Kratos AXIS Ultra Imaging spectrometer.

Results and Discussion

The TEM images in Figure 2a−c show nanocluster arrays that have been created by spin-casting a micellar solution with different metal loading ratios onto a planar substrate followed by oxygen plasma etching to remove the polymer thin film. These images illustrate the effect of the metal loading ratio on the size and spacing of the metal nanocluster arrays. In each of these images, PS/PAA (16.4/4.5) was the block copolymer and $FeCl_3$ was the selected metal salt. In Figure 2a, $FeCl_3$ was added to the block copolymer micellar solution at a loading ratio of ~0.3, leaving an excess of carboxylic acid groups relative to the amount of iron cation. In Figure 2a, the iron oxide nanoclusters have diameters of 8 ± 0.7 nm, center-to-center spacings of $\sim 40 \pm 4$ nm, and an areal density of 8×10^{10} nanoclusters cm^{-2}. In Figure 2b, the $FeCl_3$ loading ratio is increased to ~5.4; i.e., there is a significant excess of iron compared to the available carboxylic acid groups. In this image, the iron oxide nanoclusters have diameters of 16.0 ± 1.6 nm, center-to-center spacings of $\sim 45 \pm 4$ nm, and an areal density of $\sim 6 \times 10^{10}$ nanoclusters cm^{-2}. The diameter of the iron oxide nanoclusters approximately doubles as a result of the increased $FeCl_3$ loading ratio. The center-to-center spacing increases only slightly due to the increased metal loading ratio, and the variation roughly corresponds to the increase in the diameter of the nanoclusters. In Figure 2c, the $FeCl_3$ loading ratio is increased to ~15, and the iron oxide nanoclusters have diameters of 16.2 ± 1.1 nm, center-to-center spacings of $\sim 45 \pm 4$ nm, and an areal density of roughly 6×10^{10} nanoclusters cm^{-2}. By comparing the nanocluster arrays formed from an $FeCl_3$ loading ratio of 5.4 versus an $FeCl_3$ loading ratio of 15, it is clear that very little change occurs in the size or spacing of the metal nanocluster arrays, owing to the saturation of the loading capacity of the micelles. This result is supported by our observation of undissolved $FeCl_3$ precipitate remaining in the solutions with a metal loading ratio of 15, while no $FeCl_3$ precipitate remains in the solutions with a metal loading ratio of 0.3. A summary of the data for Figure 2a−c is shown in Table 1. By varying the metal loading ratio in solution, we have demonstrated the ability to exhibit a degree of control over the diameter of the metal nanoclusters that are formed at essentially constant spacing.

From the TEM images in Figure 2, it is apparent that the nanoclusters have a higher contrast around the exterior and considerably less contrast within the center of the nanocluster. We feel confident that this effect is caused by phase contrast in TEM imaging and is not

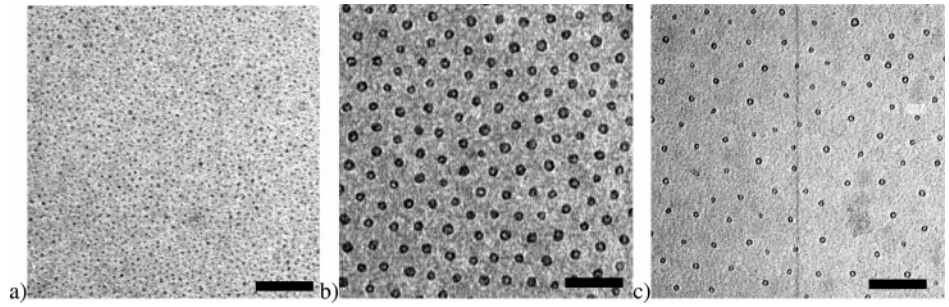

Figure 3. TEM images of iron oxide nanocluster arrays synthesized from micellar thin films with an $FeCl_3$ loading ratio of 5.4 and PS/PAA with a molecular weight of (a) 11/1.2, (b) 16.4/4.5, and (c) 66.5/4.5. Scale bar = 100 nm.

Table 2. Effect of Varying the Molecular Weight of PS/PAA on Diameter, Center-to-Center Spacing, and Areal Density of Iron Oxide Nanocluster Arrays

PS (g/mol)	PAA (g/mol)	hydrodynaic radius (R_h, nm)	diameter (nm)	C-to-C spacing (measured)[a] (nm)	(FFT)[b] (nm)	areal density (parts/cm^2)
11 000	1200	27	4.7 ± 0.6	13 ± 1.7	12	3.0×10^{11}
16 400	4500	44	16.0 ± 1.6	44.9 ± 4.0	39.5	6.0×10^{10}
66 500	4500	96	11.2 ± 1.1	57.6 ± 8.2	56	4.3×10^{10}

[a] From TEM images. [b] Determined from fast Fourier transfrom (FFT) of TEM image.

representative of the actual structure of our nanoclusters. Because these nanoclusters offer very little amplitude contrast, we are forced to take steps to increase the contrast in order to produce useful images. We accomplish this by underfocusing our sample in order to image the nanoclusters using phase contrast. When the nanoclusters are overfocused, the center of the nanoclusters appears dark and the exterior appears bright, which is a common indicator of phase contrast effects. When the nanoclusters are in focus, this effect is eliminated, but the images are extremely difficult to view due to the lack of contrast. This explanation is also confirmed by the annular dark field (ADF) image of the nanoclusters, which is shown subsequently in Figure 6b. If the nanoclusters were hollow, we would observe a bright ring with a dark center for each nanocluster in the ADF image; however, it is clear from Figure 6b that each nanocluster appears as a uniform bright circle. We also imaged these nanoclusters using AFM (image not shown), which confirmed that the nanoclusters were approximately spherical in shape and did not contain a cavity as the TEM images in Figure 2 might suggest.

We also characterized the substrates using X-ray photoelectron spectroscopy (XPS) to determine the chemical composition of the nanoclusters. We found that the nanoclusters exhibited an Fe($2p_{3/2}$) peak at ~711.7 eV and an O(1s) peak at ~530.7 eV. Comparing these values to literature values for various iron oxides, we are able to conclude that the nanoclusters are either Fe_2O_3 [Fe($2p_{3/2}$) ~ 710.9−711.6 eV and O(1s) ~ 529.6−530.3 eV] or FeOOH [Fe($2p_{3/2}$) ~ 711.0−711.8 eV and O(1s) ~ 530.1−530.5 eV for the oxide oxygen, O(1s) ~ 531.4−531.8 eV for the hydroxide oxygen],[20] or a combination of the two species. Because our nanoclusters are on silicon oxide, the O(1s) peak caused by the Si−O bond makes it extremely difficult to examine more closely the O(1s) peak associated with the nanoclusters to determine whether there are two different oxygen peaks.

The TEM images in Figure 3a−c demonstrate the effect of the molecular weight of PS/PAA on the size and spacing of the PAA domains and consequently on the size and spacing of the resulting nanoclusters. In Figure 3a, micelles formed from PS/PAA (11.0/1.2) with an $FeCl_3$ loading ratio of 5.4 led to iron oxide nanoclusters with diameters of 4.7 ± 0.6 nm, center-to-center spacings of 13 ± 1.7 nm, and density of ~3×10^{11} nanoclusters cm^{-2}. Figure 3b shows iron oxide nanoclusters with diameters of 16 ± 1.6 nm, center-to-center spacings of ~45 ± 4 nm, and density of ~6×10^{10} nanoclusters cm^{-2} that resulted from similar processing conditions for the case of the PS/PAA (16.4/4.5) copolymer. At constant loading ratio, decreasing the molecular weight of the PAA block leads to smaller nanoclusters, while decreasing the length of the PS block leads to smaller center-to-center spacing. Micelles of PS/PAA (66.5/4.5), again using a loading ratio of 5.4, were used to create iron oxide nanoclusters with diameters of 11.2 ± 1.1 nm, center-to-center spacings of 57.6 ± 8.2 nm, and a two-dimensional density of ~4×10^{10} nanoclusters cm^{-2}. Increasing the PS segment of the block copolymer 4-fold enlarged the center-to-center spacing of the PAA domains by ~30% (Figure 3b,c), and even though the PAA block length remained constant (M = 4500 g/mol), the cluster size also decreased (from 16 to 11 nm). These trends result from a decrease in aggregation number of the micelles caused by the increase in the molecular weight of the PS segment, a result that has been previously shown by Khougaz et al.[21] The three TEM images in Figure 3 demonstrate a method for controlling the size and spacing of the PAA micellar domains, which leads to control over the size and spacing of metal nanocluster arrays, as summarized in Table 2.

The variation of center-to-center spacing between the metal nanoclusters caused by the alteration of the block copolymer molecular weight also correlated with changes in the size of the micelles in solution, as verified by DLS. An average hydrodynamic radius was determined for each micellar solution, and the results are shown in Table 2. The average hydrodynamic radii were 27, 44, and 96 nm for the PS/PAA (11/1.2), PS/PAA (16.4/4.5), and the PS/PAA (66.5/4.5) systems, respectively. A scaling relationship for the total micellar radius, specific to the regime where micelles have corona segments much longer than core segments, was previously developed by Halperin.[22] This scaling relationship shows that the total micellar radius (R) scales as $(N_{PAA})^{4/25}(N_{PS})^{3/5}$, where N_{PAA} denotes the number of repeat units of the PAA segment and N_{PS} denotes the number of repeat units of the PS segment. Our hydrodynamic radius data

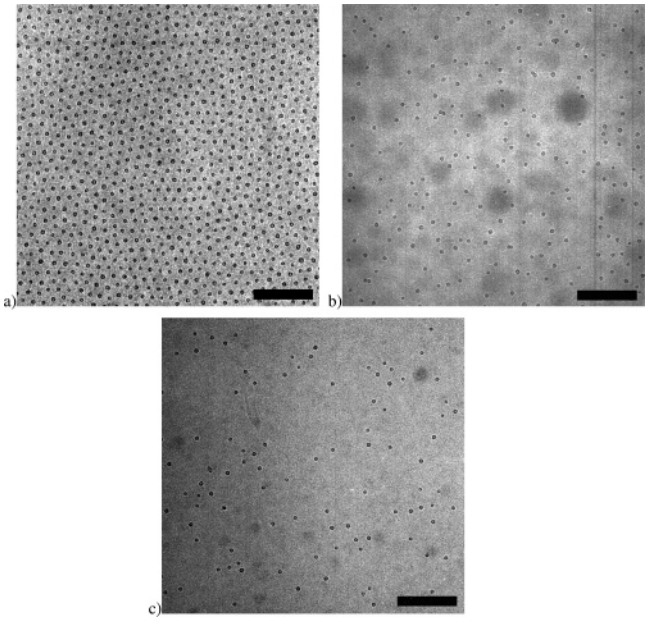

Figure 4. TEM images of iron oxide nanocluster arrays synthesized from micellar thin films using PS/PAA (16.4/4.5) with an $FeCl_3$ loading ratio of 5.4 and a [PS:PS-*b*-PAA] equal to (a) 0 (no PS homopolymer), (b) 4, and (c) 10. Scale bar = 250 nm.

from DLS agree very closely with this scaling law. However, this theory also predicts that the aggregation number and the core radius of the micelles should be independent of the PS segment length in this regime, whereas we observed a decrease in the size of the core radius with increasing the PS segment length at constant PAA segment length.

Although the areal density of the PAA domains can be tailored by variation of the molecular weight (as shown in Figure 3), there is an unavoidable coupling of areal density with the size of the nanoclusters. Therefore, a more general approach allowing independent control of these two parameters was sought. By adding PS homopolymer (M_n(PS) = 8500 g/mol) to our micellar solution, as illustrated in route iii of Figure 1, we were able to vary the areal density over an order of magnitude, as demonstrated in the TEM images in Figure 4. In all three TEM images in Figure 4, the PS/PAA (16.4/4.5) copolymer was used and the $FeCl_3$ loading ratio was constant at 5.4. In Figure 4a, no PS homopolymer was added to the solution, and a density of 6×10^{10} particles cm^{-2} was achieved. In Figure 4b, PS homopolymer was added to the micellar solution at a ratio of 4 molecules of PS homopolymer per molecule of PS/PAA block copolymer ([PS:PS/PAA] = 4). This addition of PS homopolymer decreased the density by 83% to 1.1×10^{10} particles cm^{-2}. By further increasing the PS homopolymer to block copolymer ratio ([PS:PS/PAA] = 10), as shown in Figure 4c, the density decreased to 6.5×10^9 particles cm^{-2}. These results, which are summarized in Table 3, indicate that the addition of PS homopolymer was a successful methodology for varying the 2-D density over nearly an order of magnitude. At the same time, there is a clear loss of packing regularity in the resulting nanocluster arrays.

As mentioned in the Experimental Section, the addition of PS homopolymer into the micellar solution increased the viscosity of the resulting solutions significantly, and toluene dilutions were employed to facilitate processing. As a control experiment to determine whether the dilution itself somehow affected the resulting micellar array spacing, a 5 mg/mL toluene solution of PS/PAA (16.4/4.5) without PS homopolymer was spin-cast onto a substrate to create a micellar thin film to compare with the 13 mg/mL results shown in Figure 4a. The resulting TEM images (not shown) revealed nanocluster arrays that had diameters and center-to-center spacings that were identical to the arrays in Figure 4a.

Table 3. Effects of Varying the Ratio of PS Homopolymer Molecules per PS/PAA Molecule ([PS:PS/PAA]) on the Areal Density of Iron Oxide Nanocluster Arrays Synthesized from Micellar Thin Films Using PS/PAA (16.4/4.5) with an $FeCl_3$ Loading Ratio of 5.4

PS (g/mol)	PAA (g/mol)	conc of PS/PAA (mg/mL of toluene)	ratio [PS:PS/PAA]	areal density (parts/cm^2)
16 400	4500	13	*a*	6.0×10^{10}
16 400	4500	5	4	1.1×10^{10}
16 400	4500	5	10	6.5×10^9

[a] No PS homopolymer.

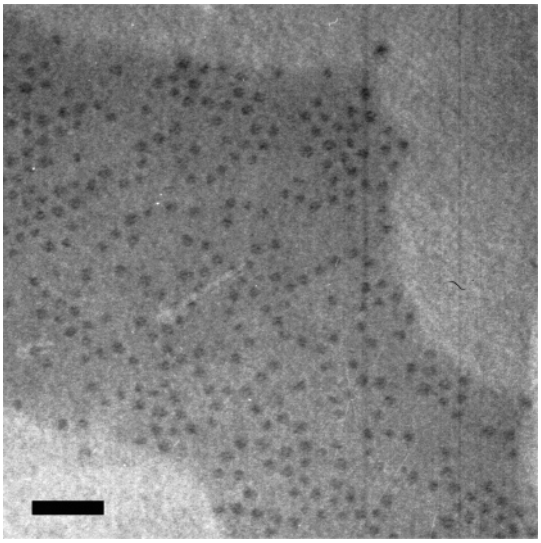

Figure 5. TEM image of Pb-containing nanocluster array formed from combining a $PbAc_2$-loaded micelle solution with an unloaded micelle solution in a 1:1 volume ratio for 1 min and then spin-casting onto a substrate. Scale bar = 100 nm.

Another useful strategy is to combine different micellar solutions, as shown in route iv from Figure 1. This novel procedure can allow for controlling the spatial density of loaded nanoreactors on the substrate or for the synthesis of multiple species metal nanocluster arrays, as described below.

Variations in the areal density of metal-loaded micelles on a substrate were achieved by combining a $PbAc_2$-loaded micelle solution (loading ratio $\sim$ 5.4) with an unloaded micelle solution in a 1:1 volume ratio for 1 min and then spin-casting the solution onto a substrate. The resulting TEM image is shown in Figure 5. It is apparent from the TEM image that the areal density of the metal nanoclusters has decreased due to the inclusion of unloaded PAA domains within the micellar thin film. By analyzing the image, we estimated the ratio of metal-loaded micelles to unloaded micelles in the thin film to be roughly 1:1, which is equal to the ratio in our initial mixture. It is interesting to note that when the $PbAc_2$-loaded micellar solution was combined with the unloaded micellar solution for an extended

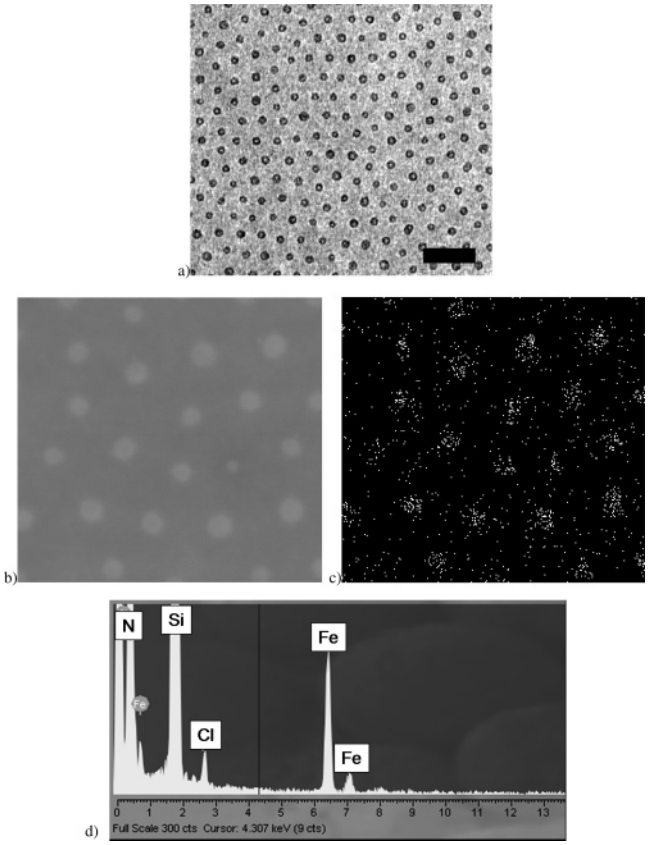

Figure 6. Characterization of a nanocluster array formed from PS/PAA (16.4/4.5) copolymer with an $FeCl_3$ loading ratio of 5.4: (a) bright field TEM image (scale bar ~ 100 nm); (b) annular dark field image obtained using STEM; (c) elemental Fe map obtained using EDX analysis with STEM; (d) EDX spectra from nanocluster obtained using STEM.

period of time (1−2 days), the thin films lacked unloaded micelles and contained only Pb-loaded micelles (images not shown). This demonstrates that there is significant diffusion and exchange of the metal species within the micellar solution and that the holding time following the combination of these micellar solutions is an important factor.

The procedure for combining different micellar solutions can also be used to create nanoclusters arrays consisting of more than one inorganic species. To characterize the nanocluster arrays with multiple metal species, we used STEM equipped with EDX analysis, which identifies elements through the detection of the characteristic energies of X-rays that are emitted from a specific atomic species when bombarded by the electron beam. The results from a typical analysis of a nanocluster array are shown in Figure 6. Using these techniques, we are able to capture an annular dark field image of the nanoclusters (shown in Figure 6b) and then create corresponding elemental maps for specific elements, shown for the case of Fe in Figure 6c. Comparing parts b and c of Figure 6, it is clear for this sample that each nanocluster contains Fe molecules. We also acquire EDX spectra for single nanoclusters by focusing the beam on each nanocluster individually, as shown in Figure 6d. This allows us to determine the composition of individual nanoclusters in a more quantitative manner. It should be noted that the large Si and N peaks seen in Figure 6d are expected and due to our use of Si_3N_4 as the substrate; an O peak is not observed because it is located within the large N peak. For each

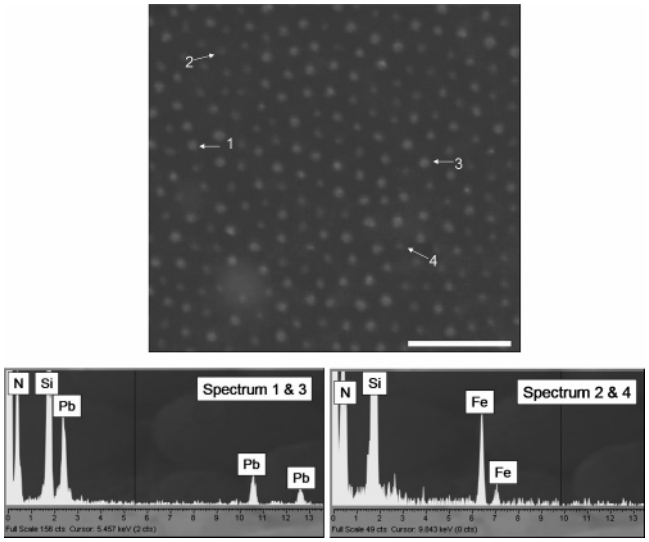

Figure 7. Annular dark field image of multispecies nanocluster array formed by combining an $FeCl_3$-loaded micellar solution (loading ratio ~ 0.3) with a $PbAc_2$-loaded micellar solution (loading ratio ~ 0.9) for 2 min, along with spectra from EDX analysis. The spectrum on the left was acquired while focusing the electron beam on the nanoclusters labeled 1 and 3 in the dark field image. The spectrum on the right was acquired while focusing the electron beam on the nanoclusters labeled 2 and 4 in the dark field image. Scale bar = 100 nm.

of the nanocluster arrays discussed below, an analysis similar to the example shown in Figure 6 was performed.

As mentioned above in the context of combining $PbAc_2$-loaded micellar solutions and unloaded micellar solutions, the contact time before spin-casting is a critical factor. To study this effect in more detail, we created a mixed micellar solution from an $FeCl_3$-loaded micellar solution (loading ratio ~ 0.3) and a $PbAc_2$-loaded micellar solution (loading ratio ~ 0.9) in a 1:1 volume ratio. Two nanocluster arrays were then created from this combined solution; one was spin-cast 2 min after the solutions were combined and the other 120 h after combination. The annular dark field image obtained from the 2 min sample is shown in Figure 7. By analyzing the elemental maps and the EDX spectra for each nanocluster (shown in Figure 7), it is evident that the nanoclusters with the higher contrast are Pb-containing nanoclusters and that the nanoclusters with lower contrast are Fe-containing nanoclusters. By examining the EDX spectra, it is also clear that each of the nanoclusters contain only one metal species; there has been no noticeable interdiffusion of metal species between micelles. In this image, 45% of the nanoclusters are iron-containing, corresponding closely to the expected value of 50% for a 1:1 volume ratio.

The resulting annular dark field image from the nanocluster array that was spin-cast 120 h after the solutions were combined is shown in Figure 8. The elemental maps as well as the EDX spectra (shown in Figure 8) reveal some nanoclusters whose compositions are nearly all one species (Fe or Pb), in addition to nanoclusters that contain both iron and lead. Figure 9 compares the nanocluster populations obtained from the 2 min and 120 h samples. Increasing the contact times for the combined micelle solutions facilitates considerable interdiffusion of Fe^{3+} and Pb^{2+} ions, resulting in nanoclusters containing multiple metal species.

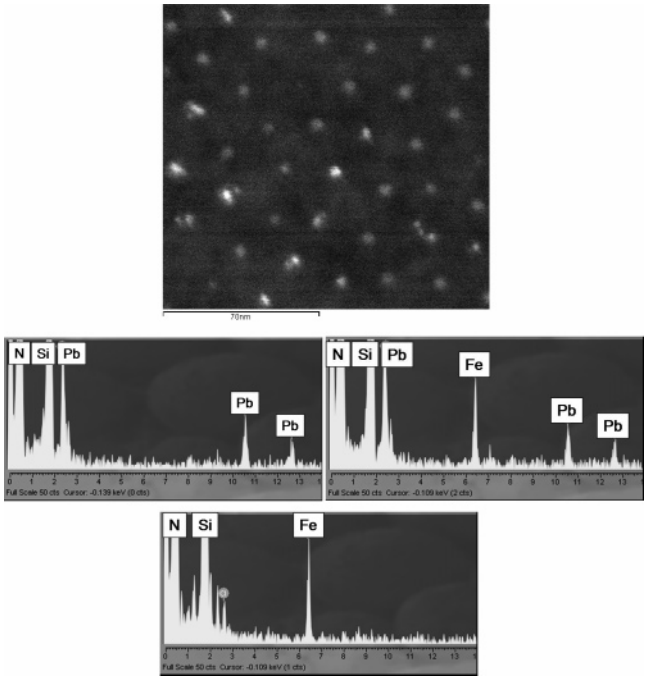

Figure 8. Annular dark field image of multispecies nanocluster array formed by combining an $FeCl_3$-loaded micellar solution (loading ratio ~ 0.3) with a $PbAc_2$-loaded micellar solution (loading ratio ~ 0.9) for 120 h, along with EDX spectra from individual nanoclusters.

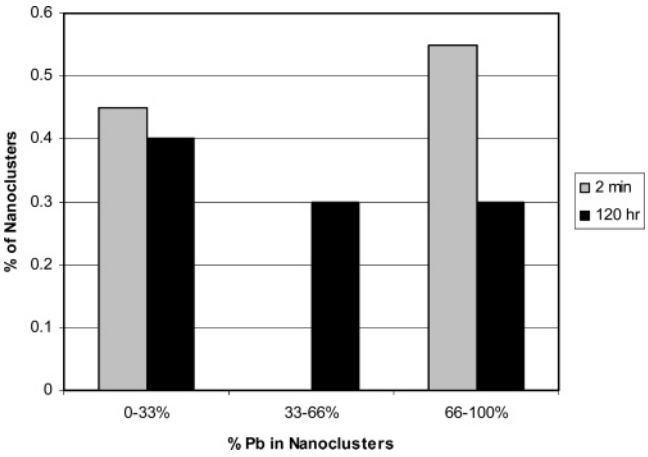

Figure 9. Comparison of the composition of multispecies nanocluster arrays formed by combining an $FeCl_3$-loaded micellar solution (loading ratio ~ 0.3) with a $PbAc_2$-loaded micellar solution (loading ratio ~ 0.9) for 2 min vs 120 h before spin-casting.

The compositions of these nanocluster arrays can also be controlled by varying the volume ratio of the combined micellar solutions. In this case, we created three separate mixed micellar solutions where an $FeCl_3$-loaded micellar solution (loading ratio ~ 0.3) was combined with a $PbAc_2$-loaded micellar solution (loading ratio ~ 0.9) in volume ratios of 1:9, 1:1, and 9:1, where the volume ratio is (mL of $FeCl_3$-loaded micelle solution: mL of $PbAc_2$-loaded micelle solution). The solutions were then spin-cast onto a substrate 120 h after they were created. After analyzing each substrate using EDX analysis, we can compare the composition of nanoclusters as a function of the initial volume ratio of the combined micellar solution, as shown in Figure 10. Variation of the volume ratio of the combined micelle solutions has a significant effect on the nanocluster

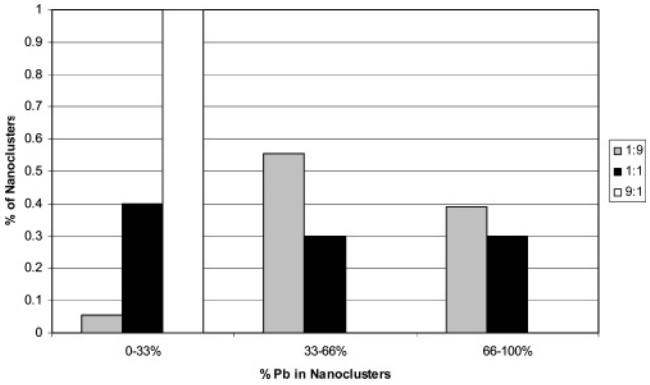

Figure 10. Comparison of the composition of multispecies nanocluster arrays formed by combining an $FeCl_3$-loaded micellar solution (loading ratio ~ 0.3) with a $PbAc_2$-loaded micellar solution (loading ratio ~ 0.9) in a volume ratio of 1:9, 1:1, and 9:1, where the ratio is (mL of $FeCl_3$-loaded micelle solution:mL of $PbAc_2$-loaded micelle solution). The solutions were spin-cast onto a substrate 120 h after they were created.

composition distribution. When the volume ratio was 1:1, we observed approximately an equal percentage of Fe-containing, Pb-containing nanoclusters, and Fe- and Pb-containing nanoclusters. When the volume ratio was changed to 9:1, we observed that nearly all of the nanoclusters were Fe-containing. When the volume ratio was 1:9, we observed ~5% of the nanoclusters were Fe-containing, 40% of the nanoclusters were Pb-containing, and 55% of the nanoclusters contained both Fe and Pb. We believe this observation is a result of the higher solubility of $FeCl_3$ in toluene compared to $PbAc_2$, which allows for higher loadings of the $FeCl_3$-loaded micelles compared to the $PbAc_2$-loaded micelles. When the micelle solutions are combined, the increased loading of the Fe-containing micelles facilitates increased exchange of the Fe^{3+} ions into Pb-loaded micelles. This results in an increased percentage of nanoclusters containing both Fe and Pb and a decreased percentage of Pb-containing micelles, as seen in the data in Figure 10.

To help understand the interdiffusion issues of these inorganic species, we used a two-step loading process to create inorganic nanocluster arrays. In this system, we created $PbAc_2$-loaded micelles (loading ratio ~ 0.9) using the PS/PAA (16.4/4.5) copolymer, and after allowing sufficient time for the Pb^{2+} ions to load, we added $FeCl_3$ (loading ratio ~ 2.1) directly into the micelle solution. After waiting 24 h, the solution was spin-cast onto a substrate to create a nanocluster array, which was characterized using EDX analysis (shown in Supporting Information). The EDX analysis showed that all of the nanoclusters contained only Fe, indicating that Fe^{3+} ions have a higher affinity for the carboxylic acid groups than Pb^{2+} ions in this system.

Conclusions

We have demonstrated the ability to vary the size, center-to-center spacing, and density of spin-cast 2-D arrays of spherical PS/PAA micelles and the subsequent inorganic nanoclusters synthesized therein. The strategies used to vary the arrays include alteration of the block copolymer molecular weight, addition of PS homopolymer, variation of the metal loading ratio in solution, and the combination of different micellar solutions. We have also demonstrated routes for the creation of metal nanocluster arrays containing multiple

metal species, in which each nanocluster contains one or more of the metal species, depending on the synthesis conditions. These routes are based on the interdiffusion and exchange of different inorganic species within micellar solutions. The strategies discussed in this work could have useful applications in the synthesis of carbon nanotube catalysts and in the construction of nanopatterned substrates for the investigation of cell attachment and function.

Acknowledgment. The Institute for Soldier Nanotechnologies (ISN) facilities and Center for Material Science and Engineering (CMSE) Shared Experimental Facilities were used extensively in this work, and the assistance of Dr. Anthony Garratt-Reed, Mike Frongillo, and Libby Shaw is gratefully acknowledged. This work was supported primarily by the MIT ISN, Project 3.17, Contract DAAD19-02-D-0002, and in part by the National Science and Defense Engineering Graduate (NDSEG) Fellowship and the MIT CMSE, NSF DMR 03-13282.

Supporting Information Available: Synthesis procedure and characterization for the diblock copolymer and EDX analysis of nanocluster arrays created from the two-step loading procedure. This material is available free of charge via the Internet at http://pubs.acs.org.

References and Notes

(1) Whitesides, G. M.; Mathias, J. P.; Seto, C. T. *Science* **1991**, *254*, 1312−1319.
(2) Hamley, I. W. *Nanotechnology* **2003**, *14*, R39−R54.
(3) Park, M.; Harrison, C.; Chaikin, P. M.; Register, R. A.; Adamson, D. H. *Science* **1997**, *276*, 1401−1404.
(4) Thurn-Albrecht, T.; Schotter, J.; Kastle, C. A.; Emley, N.; Shibauchi, T.; Krusin-Elbaum, L.; Guarini, K.; Black, C. T.; Tuominen, M. T.; Russell, T. P. *Science* **2000**, *290*, 2126−2129.
(5) Li, R. R.; Dapkus, P. D.; Thompson, M. E.; Jeong, W. G.; Harrison, C.; Chaikin, P. M.; Register, R. A.; Adamson, D. H. *Appl. Phys. Lett.* **2000**, *76*, 1689−1691.
(6) Black, C. T.; Guarini, K. W.; Milkove, K. R.; Baker, S. M.; Russell, T. P.; Tuominen, M. T. *Appl. Phys. Lett.* **2001**, *79*, 409−411.
(7) Park, M.; Chaikin, P. M.; Register, R. A.; Adamson, D. H. *Appl. Phys. Lett.* **2001**, *79*, 257−259.
(8) Cheng, J. Y.; Ross, C. A.; Thomas, E. L.; Smith, H. I.; Vancso, G. J. *Appl. Phys. Lett.* **2002**, *81*, 3657−3659.
(9) Lazzari, M.; Lopez-Quintela, M. A. *Adv. Mater.* **2003**, *15*, 1583−1594.
(10) Bates, F. S.; Fredrickson, G. H. *Annu. Rev. Phys. Chem.* **1990**, *41*, 525−557.
(11) Spatz, J. P.; Herzog, T.; Mossmer, S.; Ziemann, P.; Moller, M. *Adv. Mater.* **1999**, *11*, 149−153.
(12) Haupt, M.; Ladenburger, A.; Sauer, R.; Thonke, K.; Glass, R.; Roos, W.; Spatz, J. P.; Rauscher, H.; Riethmuller, S.; Moller, M. *J. Appl. Phys.* **2003**, *93*, 6252−6257.
(13) Spatz, J. P.; Mossmer, S.; Hartmann, C.; Moller, M.; Herzog, T.; Krieger, M.; Boyen, H. G.; Ziemann, P.; Kabius, B. *Langmuir* **2000**, *16*, 407−415.
(14) Yoo, S. I.; Sohn, B. H.; Zin, W. C.; An, S. J.; Yi, G. C. *Chem. Commun.* **2004**, 2850−2851.
(15) Fu, Q.; Huang, S. M.; Liu, J. *J. Phys. Chem. B* **2004**, *108*, 6124−6129.
(16) Yun, S. H.; Sohn, B. H.; Jung, J. C.; Zin, W. C.; Lee, J. K.; Song, O. *Langmuir* **2005**, *21*, 6548−6552.
(17) Boontongkong, Y.; Cohen, R. E. *Macromolecules* **2002**, *35*, 3647−3652.
(18) Bennett, R. D.; Xiong, G. Y.; Ren, Z. F.; Cohen, R. E. *Chem. Mater.* **2004**, *16*, 5589−5595.
(19) Sohn, B. H.; Choi, J. M.; Yoo, S. I.; Yun, S. H.; Zin, W. C.; Jung, J. C.; Kanehara, M.; Hirata, T.; Teranishi, T. *J. Am. Chem. Soc.* **2003**, *125*, 6368−6369.
(20) Data retrieved from NIST X-ray Photoelectron Spectroscopy Database: Version 2.0, located at http://nist.gov/srd/nist20.htm.
(21) Khougaz, K.; Zhong, X. F.; Eisenberg, A. *Macromolecules* **1996**, *29*, 3937−3949.
(22) Halperin, A. *Macromolecules* **1987**, *20*, 2943−2946.

MA0518555